

Title: Optimal Target Region for Subject Classification based on Amyloid PET Images

Authors: Felix Carbonell, Ph.D.¹, Alex P. Zijdenbos, Ph.D.¹, Arnaud Charil, Ph.D.¹, Marilyn Grand'Maison, MSc.¹, Barry J. Bedell, M.D., Ph.D.^{1,2}, for the Alzheimer's Disease Neuroimaging Initiative*

¹Biospective Inc., 6100 avenue Royalmount, Montreal, QC, H4P 2R2, Canada

²Research Institute of the McGill University Health Centre, 1001 Decarie Boulevard, Montreal, QC, H4A 3J1, Canada

Corresponding Author:

Barry J. Bedell, M.D., Ph.D.

Biospective Inc.

6100 avenue Royalmount

Montreal, Quebec, H4P 2R2

Canada

Phone: 1-514-283-2667

E-mail: bbedell@biospective.com

* Data used in preparation of this article were obtained from the Alzheimer's Disease Neuroimaging Initiative (ADNI) database (adni.loni.usc.edu). As such, the investigators within the ADNI contributed to the design and implementation of ADNI and/or provided data but did not participate in analysis or writing of this report. A complete listing of ADNI investigators can be found at:

http://adni.loni.usc.edu/wp-content/uploads/how_to_apply/ADNI_Acknowledgement_List.pdf

Abstract

Classification of subjects based on Amyloid PET scans is increasingly utilized in research studies and clinical practice. While qualitative, visual assessment is currently the gold-standard approach, automated classification techniques are inherently more reproducible and efficient. The objective of this work was to develop a statistical approach for the automated classification of subjects with different levels of cognitive impairment into amyloid-low ($A\beta_L$) and amyloid-high ($A\beta_H$) groups using Amyloid PET data from the Alzheimer's Disease Neuroimaging Initiative (ADNI) study.

Methods: Our framework employs an iterative, voxelwise, regularized discriminant analysis combined with a Receiver Operating Characteristic (ROC) approach that optimizes the selection of a region-of-interest (ROI) and a cutoff for automated classification of subjects into $A\beta_L$ and $A\beta_H$ groups. The robustness, spatial stability, and generalization of the resulting target ROIs were evaluated using standardized uptake value ratio (SUVR) values of ^{18}F -florbetapir PET images from healthy control, mild cognitive impairment (MCI), and Alzheimer's disease (AD) subjects participating in the ADNI study.

Results: We determined that several iterations of the discriminant analysis improved the classification of subjects into $A\beta_L$ and $A\beta_H$ groups. We found that an ROI consisting of the posterior cingulate cortex/precuneus and medial frontal cortex yielded optimal group separation and showed good stability across different reference regions and cognitive cohorts. A key step in this process was the automated determination of the cutoff value for group separation, which was dependent on the reference region employed for SUVR calculation and was shown to have a relatively narrow range across subject groups.

Conclusion: We have developed a data-driven approach for determination of an optimal target ROI and associated cutoff value for separation of subjects into $A\beta_L$ and $A\beta_H$ groups. Future work should include application of this process to other data sets, which will allow us to determine the translatability

of the optimal ROI determined in this study to other populations. Ideally, the accuracy of our target ROI/cutoff could be further validated using PET-autopsy data from large-scale studies. It is anticipated that this approach will be extremely useful for enrichment of study populations in clinical trials involving putative disease-modifying therapeutic agents for AD.

[347 words; limit = 350 words]

Keywords: Alzheimer's disease; β -amyloid; 18F-florbetapir; mild cognitive impairment; positron emission tomography

Introduction

The advent of positron emission tomography (PET) radiotracers with high specificity for β -amyloid plaques represents a paradigm shift in Alzheimer's disease (AD) research. The use of "Amyloid PET" has markedly improved our understanding of the relationship between β -amyloid pathology and cognition (1–3), brain structure (4,5), cerebral glucose metabolism (6–8), and brain connectivity (9–11). Amyloid PET is also increasingly utilized in clinical trials of putative amyloid-lowering agents for enrichment of the study population with "amyloid-positive" subjects (12–14). Finally, the approval of several fluorine-18-labeled tracers by regulatory authorities has facilitated the use of Amyloid PET as part of the clinical diagnostic work-up patients with cognitive impairment.

Conventional Amyloid PET studies employ the standardized uptake value ratio (SUVR) measure to assess subject "amyloid-status". The cerebellum has been widely utilized as the reference region for Amyloid PET studies. Clark and colleagues (15) found that whole cerebellum provided the strongest correlation between *in vivo* 18F-florbetapir SUVR and post-mortem, quantitative immunohistochemistry measures. However, the cerebellum may not satisfy the conditions for a reference region in certain cases, including familial forms of AD and cerebral amyloid angiopathy (CAA) in which cerebellar amyloid is present, leading to the use of other reference regions (*e.g.* pons, centrum semiovale, cerebral white matter) (16–19).

In addition to selection of the most suitable reference region for analysis of Amyloid PET data, determination of the appropriate target region (*i.e.* the numerator in SUVR-based analysis) and corresponding SUVR cut-off value are also matters of current debate. The choice of a suitable target region-of-interest (ROI) is crucial when performing quantitative analysis of the PET imaging data. Several Amyloid PET target ROIs have been proposed, varying from whole cortex (20) to more specific cortical regions (*e.g.* frontal, superior parietal, lateral temporal, lateral occipital, medial temporal, anterior cingulate and posterior cingulate cortex) (21–25). While these target regions have

largely been selected based on high levels of tracer binding, they are not necessary optimal for the classification of subjects into “amyloid-low” ($A\beta_L$) and “amyloid-high” ($A\beta_H$) groups (note that we prefer this terminology opposed to “amyloid-negative” and “amyloid-positive”, which requires neuropathologic confirmation). Further, the classification of subjects into $A\beta_L$ and $A\beta_H$ groups depends on the specification of a cutoff SUVR value that discriminates individuals into two populations according to the amount of tracer binding in the pre-defined target ROI. A common approach has been determination of the optimal cutoff value from control (*e.g.* cognitively normal subjects) populations (7,25–27). The main drawback of this approach is that the cutoff value is typically dependent on the SUVR distribution of the control group. As such, the objective of this work was to employ a data-driven approach to determine the target region and associated SUVR threshold to achieve maximal separation between $A\beta_L$ and $A\beta_H$ groups. In order to assess the robustness and generalization of the resulting target region, we have performed extensive testing using different subject populations and different reference regions.

Materials and Methods

Subjects and Image Acquisition

Data used in the preparation of this article were obtained from the Alzheimer's Disease Neuroimaging Initiative (ADNI) database (<http://adni.loni.usc.edu>). The ADNI was launched in 2003 by the National Institute on Aging (NIA), the National Institute of Biomedical Imaging and Bioengineering (NIBIB), the Food and Drug Administration (FDA), private pharmaceutical companies and non-profit organizations, as a \$60 million, 5-year public private partnership. The primary goal of ADNI has been to test whether serial magnetic resonance imaging (MRI), PET, other biological markers, and clinical and neuropsychological assessment can be combined to measure the progression of MCI and AD. Determination of sensitive and specific markers of very early AD progression is intended to aid researchers and clinicians to develop new treatments and monitor their effectiveness, as well as lessen the time and cost of clinical trials. ADNI is the result of efforts of many co-investigators from a broad range of academic institutions and private corporations, and subjects have been recruited from over 50 sites across the U.S. and Canada. The initial goal of ADNI was to recruit 800 subjects, but ADNI has been followed by ADNI-GO and ADNI-2. To date, these three protocols have recruited over 1500 adults, ages 55 to 90, to participate in the research, consisting of cognitively normal older individuals, people with early or late mild cognitive impairment (MCI), and people with early AD. The follow-up duration of each group is specified in the protocols for ADNI-1, ADNI-2, and ADNI-GO. Subjects originally recruited for ADNI-1 and ADNI-GO had the option to be followed in ADNI-2. For up-to-date information, see www.adni-info.org.

The subjects of this study consisted of 155 healthy control (HC) subjects, 151 early MCI subjects (EMCI), 125 late MCI subjects (LMCI), and 23 AD subjects from the ADNI study who had available 18F-florbetapir PET, 3D T1-weighted anatomical MRI, and APOE ϵ 4 genotyping. Cognitively normal subjects had Mini-Mental State Exam (MMSE) scores between 24 and 30

inclusively, a CDR of 0, were non-depressed, non-MCI, and non-demented. Subjects classified as EMCI had MMSE scores between 24 and 30 inclusively, Clinical Dementia Rating (CDR) of 0.5, a reported subjective memory concern, an absence of dementia, an objective memory loss measured by education-adjusted scores on delayed recall of one paragraph from Wechsler Memory Scale Logical Memory II, essentially preserved activities of daily living (ADL), and no impairment in other cognitive domains. LMCI subjects had the same inclusion criteria, except for the objective memory loss measured by education adjusted-scores on delayed recall of one paragraph from Wechsler Memory Scale Logical Memory II. AD subjects presented with MMSE scores ranging from 20 to 26 inclusively, a CDR of 0.5 or higher, and met the NINCDS/ADRDA criteria for probable AD.

Subject characteristics are provided in Table 1. We grouped the subjects into two cohorts in order to examine the stability of the proposed, optimal target ROI across subjects with different levels of cognitive impairment. Cohort 1 included EMCI and LMCI subjects, while Cohort 2 consisted of the combination of HC and AD subjects. A detailed description of the ADNI MRI and PET image acquisition protocols can be found at <http://adni.loni.usc.edu/methods>. ADNI studies are conducted in accordance with the Good Clinical Practice guidelines, the Declaration of Helsinki, and U.S. 21 CFR Part 50 (Protection of Human Subjects), and Part 56 (Institutional Review Boards). This study was approved by the Institutional Review Boards of all of the participating institutions. Informed written consent was obtained from all participants at each site.

Image Processing

All MRI and PET images were processed using the PIANO™ software package (Biospective Inc., Montreal, Canada). T1-weighted MRI volumes underwent image non-uniformity correction using the N3 algorithm (28), brain masking, linear spatial normalization utilizing a 9-parameter affine transformation, and nonlinear spatial normalization (29) to map individual images from native coordinate space to MNI reference space using a customized, anatomical MRI template derived from

ADNI subjects. The resulting image volumes were segmented into gray matter (GM), white matter (WM), and cerebrospinal fluid (CSF) using an artificial neural network classifier (30) and partial volume estimation (31). The gray matter density map for each subject was transformed to the same final spatial resolution (*i.e.*, re-sampled to the same voxel size and spatially smoothed) as the FDG PET data in order to account for confounding effects of atrophy in the statistical model. The cerebral mid-cortical surface (*i.e.*, the mid-point between the pia and WM) for each hemisphere was extracted to allow for surface projection of PET data using a modified version of the CLASP algorithm (32).

The 18F-florbetapir PET images underwent several pre-processing steps, including frame-to-frame linear motion correction, smoothing using a scanner-specific blurring kernel, and averaging of dynamic frames into a static image. The scanner-specific blurring kernels that were used to obtain an isotropic spatial smoothing of 8mm FWHM across all PET data were based on the work of Joshi and colleagues (33) to reduce the between-scanner differences in the ADNI multi-center study. The resulting smoothed PET volumes were linearly registered to the subject T1-weighted MRI and, subsequently, spatially normalized to reference space using the nonlinear transformations derived from the anatomical MRI registration. Voxelwise standardized uptake value ratio (SUVR) maps were generated from 18F-florbetapir PET using several reference regions, including full cerebellum (CbFull), cerebellum gray matter (CbGM), cerebellum white matter (CbWM), pons, and cerebral white matter (CWM). The cortical SUVR measures were projected onto the cortical surface, and the data from each subject was mapped to a customized surface template by non-rigid 2D surface registration for visualization purposes (34).

Subject Characteristic Analysis

A statistical analysis of subject characteristics within each cohort was performed. The clinical classification (NC, EMCI, LMCI, and AD) and APOE ϵ 4 genotype (non-carrier and carrier) were

treated as independent, binary categorical variables. Cognitive performance measures, including MMSE score and Alzheimer's Disease Assessment Scale - Cognitive Subscale (ADAS-Cog), as well as CSF $A\beta_{1-42}$ were treated as continuous variables. Associations amongst categorical variables (*e.g.* gender, clinical classification, APOE $\epsilon 4$ genotype) were determined using contingency tables, while analysis of continuous variables (*e.g.* age, 18F-florbetapir $SUVR_{WC}$, MMSE, ADAS-Cog, $A\beta_{1-42}$) was performed by analysis-of-variance (ANOVA). The statistical significance for all tests was set at $\alpha = 0.05$. All values are reported as mean \pm standard deviation.

Optimal Target ROI Definition

The mean 18F-florbetapir SUVR across the whole cerebral cortex was calculated for each subject ($SUVR_{WC}$). An initial Regularized Discriminant Analysis (RDA) (35) was performed in order to determine the optimal threshold to separate subjects into two distinct classes based on individual $SUVR_{WC}$ measurements. RDA assumes an underlying Gaussian distribution and defines discriminative functions based on the sample means and covariance matrices. RDA includes a regularization parameter that controls the degree of contraction of each individual class covariance matrix estimate (quadratic discriminant analysis [QDA]) towards the pooled (over all classes) covariance matrix (linear discriminant analysis [LDA]). As a result, RDA is a general discriminant analysis technique that includes LDA and QDA as particular cases. Individual 18F-florbetapir $SUVR_{WC}$ measurements were ranked, and cutoff values that separated measures into two different classes were defined. The RDA defined the contraction parameter that yielded the maximal accuracy at each cutoff. The optimal cutoff value was then determined via Receiver Operating Characteristic (ROC) analysis. Based on this $SUVR_{WC}$ cutoff value, subjects were designated as $A\beta_L$ or $A\beta_H$.

This preliminary classification of subjects served to initialize an automated, iterative, voxelwise RDA to optimize the selection of a set of regions-of-interest (ROIs) and a cutoff value for automated

re-classification of $A\beta_L$ and $A\beta_H$ subjects (see flow diagram in Figure 1). Specifically, at the first iteration, an RDA was performed at every cortical voxel to produce maps of accuracy, specificity, and sensitivity (relative to the current subject's classification as $A\beta_L$ or $A\beta_H$). These maps were thresholded using a non-parametric permutation approach for control of multiple comparisons (36). The conjunction (*i.e.* intersection) of the resulting thresholded maps served to define a single, composite ROI which maximized the accuracy, specificity, and sensitivity. The average 18F-florbetapir SUVR was then computed over this composite ROI ($SUVR_{ROI}$) for each subject. Another round of RDA was performed based on the $SUVR_{ROI}$ data, rather than the voxelwise values, and an optimal $SUVR_{ROI}$ cutoff value was determined via ROC analysis. Based on this new cutoff value, the subjects were re-classified into $A\beta_L$ and $A\beta_H$ groups. Using this approach, subjects are re-labeled as $A\beta_L$ or $A\beta_H$ based on RDA analysis from a data-driven, composite ROI and associated optimal cutoff value. The entire process was then iterated until the subject classification remained stable.

Results

Subject Characteristics

The analysis of subject characteristics from Cohort 1 revealed no statistically significant association between the clinical classification (EMCI vs. LMCI) and the APOE $\epsilon 4$ genotype ($p = 0.08$). Similarly, there was no significant association between gender and clinical classification ($p = 0.82$). In contrast, there was a statistically significant age difference between EMCI and LMCI subjects ($p = 0.0017$). The initial whole cortex SUVR measurements ($SUVR_{WC}$ with full cerebellum as a reference region) also showed a statistically significant difference ($p = 0.002$) between EMCI (1.21 ± 0.17) and LMCI (1.28 ± 0.18) subjects. Statistical analysis of the cognitive measures and CSF biomarkers reported in Table 1 revealed strong, statistically significant differences ($p < 0.0001$) between EMCI and LMCI subjects. Analysis of data from Cohort 2 subjects revealed a statistically significant association ($p < 0.0001$)

between clinical classification (NC vs. AD) and APOE $\epsilon 4$ genotype, but no significant association ($p = 0.24$) with gender. Similar to Cohort 1, the initial $SUVR_{WC}$ measurements were significantly higher ($p < 0.001$) in the AD group (1.36 ± 0.20) than in the NC group (1.17 ± 0.15). The cognitive performance measures and CSF $A\beta_{1-42}$ showed strong, statistically significant differences ($p < 0.0001$) between NC and AD subjects.

Optimal Target ROI

The initial RDA and ROC analysis based on the whole cortical $SUVR$ ($SUVR_{WC}$; full cerebellum as reference region) for Cohort 1 yielded a cutoff value of 1.20. The top row in Figure 2 shows the distribution and estimated probability density function of the $SUVR_{WC}$ values. This analysis separated Cohort 1 into two groups, consisting of 131 $A\beta_L$ with $SUVR_{WC}$ values less or equal than 1.20, and 145 $A\beta_H$ subjects with $SUVR_{WC}$ values greater than 1.20. This preliminary classification was used to initialize the voxelwise RDA that generated the accuracy, specificity, and sensitivity maps shown in Figure 3. Permutation testing with a multiple comparison correction approach yielded respective thresholds of 0.80, 0.86, and 0.83, which revealed the bilateral precuneus and medial frontal cortex as regions with statistically significant, high values of accuracy, specificity, and sensitivity. The conjunction analysis (*i.e.* intersection) of the thresholded maps produced a composite target ROI (top row in Figure 4) corresponding to the first iteration of our automated classification process. The ROC analysis over the $SUVR_{ROI}$ values corresponding to this composite target region yielded an $SUVR_{ROI}$ cutoff value of 1.27.

Three additional iterations were performed in order to obtain the definitive composite target ROI (bottom row in Figure 4) that maximized the separation of Cohort 1 subjects into the $A\beta_L$ and $A\beta_H$ groups. The resulting distribution and estimated probability density function of the optimal target $SUVR_{ROI}$ values are also shown in Figure 2. The sample size distribution of the two groups and the

optimal cutoff values obtained in each iteration are provided in Table 2. In order to illustrate the dynamic allocation of subjects into the two groups during the iterative process, Table 2 also presents the accuracy, specificity, and sensitivity values of the resulting classification with respect to the initial labeling, based on $SUVR_{WC}$ (Acc-WC, Spec-WC, and Sens-WC), and with respect to the preceding iteration (Acc-Iter, Spec-Iter, and Sens-Iter). Note that during the first iteration, 149 subjects were allocated to the $A\beta_H$ group, including 97.2% (*i.e.* Sens-WC = 0.972) out of the 145 $A\beta_H$ subjects from the initial classification. By the fourth iteration, only 141 subjects were allocated into the $A\beta_H$ group, including 93.8% of the original 145 subjects in that particular group. Interestingly, none of the 128 subjects initially classified as $A\beta_L$ changed groups through subsequent iterations. The definitive classification into 135 $A\beta_L$ and 141 $A\beta_H$ subjects based on the cutoff value of 1.24 produced accuracy, specificity, and sensitivity values of 0.985, 0.970 and 1.000, respectively.

Given the lack of an autopsy gold-standard, we correlated the $SUVR_{ROI}$ values in the optimal composite target ROI with the CSF $A\beta_{1-42}$ in the subset of subjects that had this measure available. The $SUVR_{ROI}$ values in the optimal composite target ROI strongly correlated ($p < 0.0001$) with the CSF $A\beta_{1-42}$ across the subjects corresponding to Cohort 1 (Spearman correlation coefficient $r = -0.7361$). The average CSF $A\beta_{1-42}$ was significantly smaller ($p < 0.0001$) in the $A\beta_H$ group (133.54 ± 23.19) than in the $A\beta_L$ group (207.98 ± 41.32).

Analogous to Figure 4, Supplementary Figure 1 shows the composite ROI for the optimal separation of the Cohort 1 MCI subjects into $A\beta_L$ and $A\beta_H$ groups using CbGM, CbWM, pons, and CWM as reference regions. The bilateral precuneus and medial frontal cortex define a composite target ROI that remains stable across the five different reference regions employed in this study (Figure 4 and Supplementary Figure 1).

Figure 5 shows the composite target ROI resulting from our iterative classification process applied to Cohort 2 using the full cerebellum as a reference region. The optimal composite target ROI

included bilateral precuneus, medial frontal cortex, and regions in the temporal-parietal cortex. In this case, only three iterations were required to segregate this population into 108 $A\beta_L$ and 70 $A\beta_H$ subjects with a cutoff value of 1.29, and with accuracy, specificity and sensitivity of 0.983, 0.981, and 0.985, respectively.

Similar to Cohort 1, the $SUVR_{ROI}$ values corresponding to Cohort 2 subjects showed a statistically significant ($p < 0.0001$) correlation with CSF $A\beta_{1-42}$ ($r = -0.7507$). The average CSF $A\beta_{1-42}$ values were significantly smaller ($p < 0.0001$) in the $A\beta_H$ group (140.01 ± 37.05) compared to the $A\beta_L$ group (215.31 ± 41.58).

Comparison with Anatomical Target ROI

The performance of our data-driven composite target ROI and associated, automated cutoff has been compared with subject classification based on ^{18}F -florbetapir $SUVR$ values (with full cerebellum as a reference region) obtained from an anatomically pre-defined composite ROI (Anat-ROI). Specifically, this ROI included anatomically-parcellated regions of the precuneus, posterior cingulate, and medial frontal cortex (cutoff value = 1.10), which has been one of the most commonly used target ROIs for discriminating subjects with low and high levels of β -amyloid (15,25,37). The cutoff value of 1.10 over the $SUVR_{Anat-ROI}$ values split Cohort 1 into 111 $A\beta_L$ and 165 $A\beta_H$ subjects. A discriminant analysis based on this classification demonstrated an accuracy of 0.942, specificity of 0.981, and sensitivity of 0.915, which is a clear decrease in discriminative power as compared to the accuracy of 0.985 achieved with our data-driven composite target ROI and cutoff of 1.24. A contingency table analysis between both classifications showed an agreement of 91.3%, explained by an identical classification of 111 $A\beta_L$ and 141 $A\beta_H$ subjects. Similarly, the cutoff of 1.10 over the $SUVR_{Anat-ROI}$ values split Cohort 2 into 100 $A\beta_L$ and 78 $A\beta_H$ subjects, with accuracy, specificity, and sensitivity of 0.966, 0.970, and 0.961,

respectively. This classification showed a 94.3% agreement with our automated, data-driven classification.

Stable Target ROIs

The intersection of the composite ROIs corresponding to the five different reference regions produced an optimal, stable composite ROI for the Cohort 1 subjects. This stable target ROI (ROI-Cohort 1) is shown in the top row of Figure 6. The high discriminative power (average accuracy of 0.987) recovered with ROI-Cohort 1 (see details in Supplementary Table 1) confirms that this target ROI is indeed stable across the five different reference regions. Similar to Cohort 1, optimal composite ROIs were generated for Cohort 2 using CbGM, CbWM, pons, and CWM as reference regions (Supplementary Figure 2). Correspondingly, the intersection of the composite ROIs for these five reference regions produced a stable target ROI for Cohort 2 (ROI-Cohort 2), which is shown in the middle row of Figure 6. The recovered discriminative parameters and corresponding cutoff values for ROI-Cohort 2 are also shown in Supplementary Table 1.

In order to determine if a “generalized” target ROI could be applied to both Cohort 1 and Cohort 2 with good performance characteristics, we intersected the target ROIs corresponding to the two cohorts. This composite ROI (ROI-Combined) is shown in the bottom row of Figure 6. The data in Supplementary Table 1 demonstrates that the ROI-Combined yields similar results to the ROI from the individual cohorts. This observation suggests that it is primarily the medial frontal cortex and posterior cingulate/precuneus driving the classification, and the lateral cortical regions in ROI-Cohort 2 do not have substantial influence on the group separation.

Discussion

In this work, we have introduced a new statistical framework for determining an optimal target region that best segregates subjects according to their level of 18F-florbetapir amyloid PET tracer binding. This approach involves iterative generation of voxelwise maps of accuracy, specificity, and sensitivity, which are combined with a multiple comparisons criteria approach to produce the desired optimal target region. A subsequent ROC analysis over the target region SUVR measure yields the corresponding optimal cutoff value. The performance of this approach was evaluated on two different cohorts of subjects from the ADNI study, as well as SUVR measures computed with multiple, different reference regions.

Our approach was able to converge to a generalized composite target ROI (ROI-Combined in Figure 6), which included regions in the posterior cingulate cortex/precuneus and medial frontal cortex, and shows good stability across the two different cognitive cohorts and the five different reference regions. Our results are in agreement with those reported by Camus *et al.* (20), which showed that SUVR values in the posterior cingulate cortex, precuneus, and medial frontal cortex were statistically significant higher in AD patients than in MCI and HC subjects. Correspondingly, the SUVR values associated with the areas comprising our optimal target ROI have been reported to be highly correlated with β -amyloid burden as measured by both immunohistochemistry and neuritic plaque density (15).

The initial step in our iterative process was to apply a RDA to the individual $SUVR_{wc}$ measurements. The global cortex florbetapir SUVR has been used by Camus *et al.* (20) to differentiate between patients with MCI and mild AD from HC subjects, reaching a sensitivity of 0.932 and specificity of 0.905 relative to pre-established visual assessment of the PET scans. Similarly, whole brain neocortical SUVR measurements of 18F-florbetaben were used for discriminating AD versus HC, with a sensitivity of 0.97 and specificity of 0.84 (24). In this work, we have demonstrated that the accuracy, sensitivity, and specificity achieved with the initial global cortex SUVR measurements can

be improved by iterating the discriminative process and refining the optimal target ROI. As part of our work, we have found that the global cortical SUVR can be replaced by other measures (*e.g.* visual assessment) for the initial classification and still converge to similar results.

A key step in our statistical framework is determination of the cutoff value for classification of subjects based on the optimal target ROI SUVR measurements. Typically, cutoff values are selected based on the comparison of the SUVR distribution of a cognitively normal population with the abnormal population under study (4,20,25,27,37,38). The main drawback of this approach is that there is no guarantee that cognitively normal subjects will be free of β -amyloid accumulation, which can only be confirmed either by the visual assessment of an experienced rater or by post-mortem neuropathology. A cutoff value of 1.10 has been proposed following a 24-month autopsy study which confirmed that all the subjects without β -amyloid plaques (by silver stain plaque density scores) had SUVR values less than 1.10 (37). The same cutoff value has been used to differentiate between normal scans from a population of cognitively normal young participants from abnormal scans visually assessed by experienced raters (25). Similarly, a cutoff value of 1.12 was used in a routine clinical environment to differentiate MCI/mild AD patients from healthy control subjects (20). A recent meta-analysis showed that SUVR cutoff values separating β -amyloid positive and negative subjects vary from 1.1 to 1.6, with a mean of approximately 1.3 (39). However, we have shown in this study that the SUVR cutoff value depends not only on the distribution of the SUVR measurements across the populations, but also on the selected reference region. Most of the studies included in the aforementioned meta-analysis (39) employed the full cerebellum as a reference region. To the best of our knowledge, our study is the first to determine an optimal target ROI and corresponding SUVR cutoff value derived from an exploration of several reference regions. A distinctive aspect of our approach is that we have employed ROC analysis for automated, unbiased determination of the optimal

cutoff value and allowed for re-labeling of subject classification during the iterative process to achieve maximal group separation.

Conclusions

We have developed a data-driven approach for determination of an optimal target ROI and associated cutoff value for separation of subjects into $A\beta_L$ and $A\beta_H$ groups. The accurate classification of subjects as $A\beta_L$ and $A\beta_H$ is vital to understand the relationship between β -amyloid burden and various other measures, including cognitive performance, cerebral blood flow, glucose metabolism, brain atrophy, and brain connectivity. Further, the relationship between the presence of β -amyloid in “cognitively normal” subjects and the future development of cognitive impairment and dementia is actively being pursued as part of long-term, longitudinal, natural history studies. Future work should include application of this process to other data sets, which will allow us to determine the translatability of the optimal ROI determined in this study to other populations. While we have shown a strong correlation between our classification and CSF $A\beta_{1-42}$, it would, of course, be ideal to validate the accuracy of our target ROI/cutoff on large-scale PET-autopsy study data. Ultimately, it is anticipated that this approach will be exceptionally useful for enrichment of study populations in natural history research studies and in clinical trials involving putative disease-modifying therapeutic agents for AD.

Acknowledgements

This work was supported, in part, by the National Research Council Canada – Industrial Research Assistance Program (NRC-IRAP).

Data collection and sharing for this project was funded by the Alzheimer's Disease Neuroimaging Initiative (ADNI) (National Institutes of Health Grant U01 AG024904) and DOD ADNI

(Department of Defense award number W81XWH-12-2-0012). ADNI is funded by the National Institute on Aging, the National Institute of Biomedical Imaging and Bioengineering, and through generous contributions from the following: Alzheimer's Association; Alzheimer's Drug Discovery Foundation; BioClinica, Inc.; Biogen Idec Inc.; Bristol-Myers Squibb Company; Eisai Inc.; Elan Pharmaceuticals, Inc.; Eli Lilly and Company; F. Hoffmann-La Roche Ltd and its affiliated company Genentech, Inc.; GE Healthcare; Innogenetics, N.V.; IXICO Ltd.; Janssen Alzheimer Immunotherapy Research & Development, LLC.; Johnson & Johnson Pharmaceutical Research & Development LLC.; Medpace, Inc.; Merck & Co., Inc.; Meso Scale Diagnostics, LLC.; NeuroRx Research; Novartis Pharmaceuticals Corporation; Pfizer Inc.; Piramal Imaging; Servier; Synarc Inc.; and Takeda Pharmaceutical Company. The Canadian Institutes of Health Research is providing funds to support ADNI clinical sites in Canada. Private sector contributions are facilitated by the Foundation for the National Institutes of Health (www.fnih.org). The grantee organization is the Northern California Institute for Research and Education, and the study is coordinated by the Alzheimer's Disease Cooperative Study at the University of California, San Diego. ADNI data are disseminated by the Laboratory for Neuro Imaging at the University of Southern California.

Disclosure/conflict of interest

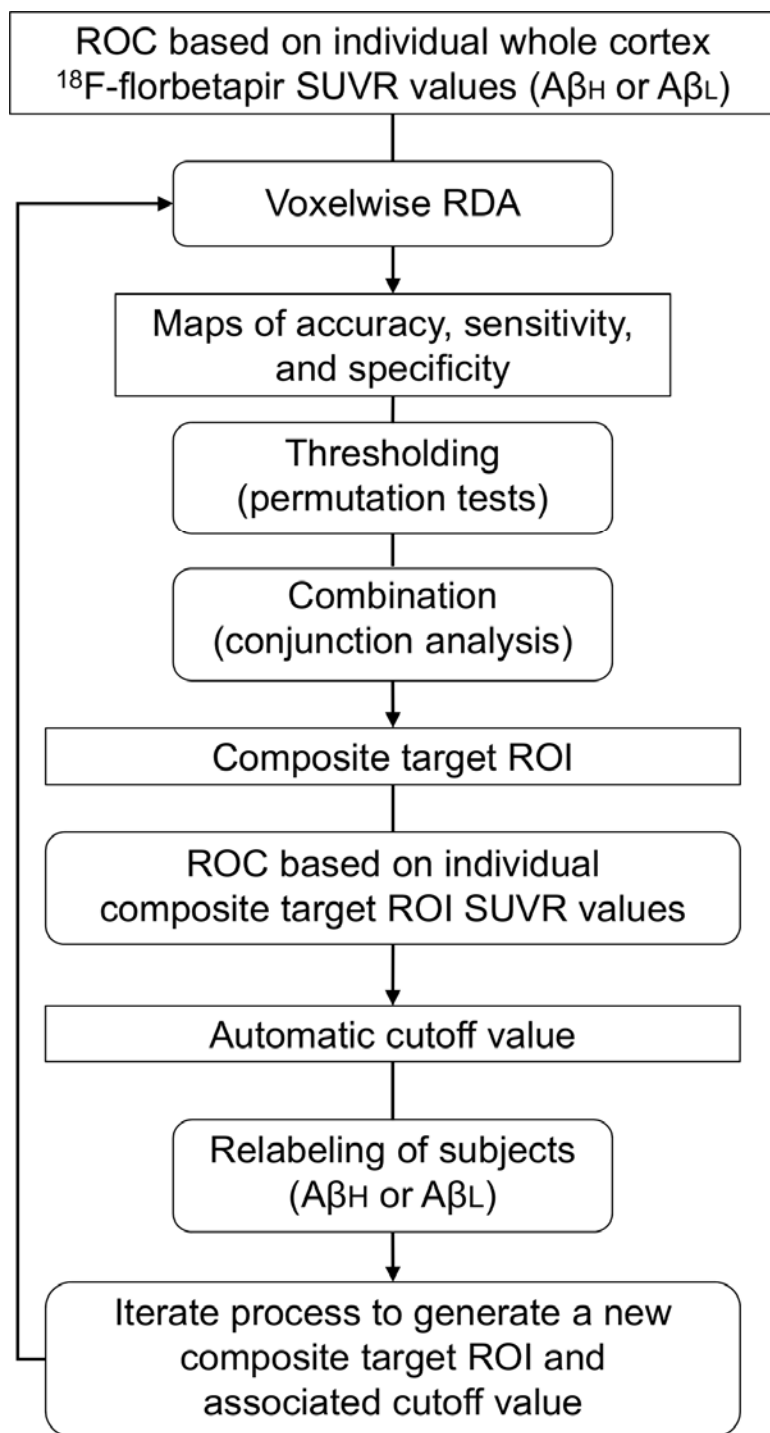
F.C., A.P.Z., and A.C. are employees of Biospective. A.P.Z. and B.J.B. are shareholders of Biospective.

References

1. Nordberg A, Carter SF, Rinne J, et al. A European multicentre PET study of fibrillar amyloid in Alzheimer's disease. *Eur J Nucl Med Mol Imaging*. 2013;40:104-114.
2. Pike KE, Savage G, Villemagne VL, et al. β -amyloid imaging and memory in non-demented individuals: Evidence for preclinical Alzheimer's disease. *Brain*. 2007;130:2837-2844.
3. Villemagne VL, Burnham S, Bourgeat P, et al. Amyloid β deposition, neurodegeneration, and cognitive decline in sporadic Alzheimer's disease: a prospective cohort study. *Lancet Neurol*. 2013;12:357-367.
4. Chételat G, Villemagne VL, Bourgeat P, et al. Relationship between atrophy and beta-amyloid deposition in Alzheimer disease. *Ann Neurol*. 2010;67:317-324.
5. Bourgeat P, Chételat G, Villemagne VL, et al. Beta-amyloid burden in the temporal neocortex is related to hippocampal atrophy in elderly subjects without dementia. *Neurology*. 2010;74:121-127.
6. Lowe VJ, Kemp BJ, Jack CR, et al. Comparison of 18F-FDG and PiB PET in cognitive impairment. *J Nucl Med*. 2009;50:878-886.
7. Devanand DP, Mikhno A, Pelton GH, et al. Pittsburgh compound B (11C-PIB) and fluorodeoxyglucose (18 F-FDG) PET in patients with Alzheimer disease, mild cognitive impairment, and healthy controls. *J Geriatr Psychiatry Neurol*. 2010;23:185-198.
8. Kadir A, Almkvist O, Forsberg A, et al. Dynamic changes in PET amyloid and FDG imaging at different stages of Alzheimer's disease. *Neurobiol Aging*. 2012;33:198.e1–198.e14.
9. Myers N, Pasquini L, Göttler J, et al. Within-patient correspondence of amyloid- β and intrinsic network connectivity in Alzheimer's disease. *Brain*. 2014;137:2052-2064.
10. Drzezga A, Becker JA, Van Dijk KRA, et al. Neuronal dysfunction and disconnection of cortical hubs in non-demented subjects with elevated amyloid burden. *Brain*. 2011;134:1635-1646.
11. Carbonell F, Charil A, Zijdenbos AP, Evans AC, Bedell BJ. β -Amyloid is associated with aberrant metabolic connectivity in subjects with mild cognitive impairment. *J Cereb Blood Flow Metab*. 2014;34:1169-1179.
12. Cummings JL. Biomarkers in Alzheimer's disease drug development. *Alzheimer's Dement*. 2011;7:e13-44.
13. Jagust W, Reed B, Mungas D, Ellis W, Decarli C. What does fluorodeoxyglucose PET imaging add to a clinical diagnosis of dementia? *Neurology*. 2007;69:871-877.

14. Albert MS, DeKosky ST, Dickson D, et al. The diagnosis of mild cognitive impairment due to Alzheimer's disease: recommendations from the National Institute on Aging-Alzheimer's Association workgroups on diagnostic guidelines for Alzheimer's disease. *Alzheimer's Dement*. 2011;7:270-279.
15. Clark CM, Schneider JA, Bedell BJ, et al. Use of florbetapir-PET for imaging beta-amyloid pathology. *JAMA*. 2011;305:275-283.
16. Edison P, Hinz R, Ramlackhansingh A, et al. Can target-to-pons ratio be used as a reliable method for the analysis of [11C]PIB brain scans? *Neuroimage*. 2012;60:1716-1723.
17. Wong DF, Rosenberg PB, Zhou Y, et al. In vivo imaging of amyloid deposition in Alzheimer disease using the radioligand 18F-AV-45 (florbetapir F 18). *J Nucl Med*. 2010;51:913-920.
18. Fleisher AS, Chen K, Liu X, et al. Using positron emission tomography and florbetapir F18 to image cortical amyloid in patients with mild cognitive impairment or dementia due to Alzheimer disease. *Arch Neurol*. 2011;68:1404-1411.
19. Chen K, Roontiva A, Thiyyagura P, et al. Improved power for characterizing Amyloid- β PET changes and evaluating amyloid-modifying treatments with a cerebral white matter reference region. *J Nucl Med*. 2015;56:560-566.
20. Camus V, Payoux P, Barré L, et al. Using PET with 18F-AV-45 (florbetapir) to quantify brain amyloid load in a clinical environment. *Eur J Nucl Med Mol Imaging*. 2012;39:621-631.
21. Rowe C, Ackerman U, Browne W. Imaging of amyloid β in Alzheimer's disease with 18 F-BAY94-9172, a novel PET tracer: proof of mechanism. *Lancet Neurol*. 2008;7:129-135.
22. Vandenberghe R, Van Laere K, Ivanoiu A, et al. 18F-flutemetamol amyloid imaging in Alzheimer disease and mild cognitive impairment: a phase 2 trial. *Ann Neurol*. 2010;68:319-329.
23. Barthel H, Gertz H-J, Dresel S, et al. Cerebral amyloid- β PET with florbetaben (18F) in patients with Alzheimer's disease and healthy controls: a multicentre phase 2 diagnostic study. *Lancet Neurol*. 2011;10:424-435.
24. Villemagne VL, Ong K, Mulligan RS, et al. Amyloid imaging with (18)F-florbetaben in Alzheimer disease and other dementias. *J Nucl Med*. 2011;52:1210-1217.
25. Joshi AD, Pontecorvo MJ, Clark CM, et al. Performance characteristics of amyloid PET with florbetapir F 18 in patients with alzheimer's disease and cognitively normal subjects. *J Nucl Med*. 2012;53:378-384.
26. Landau SM, Harvey D, Madison CM, et al. Comparing predictors of conversion and decline in mild cognitive impairment. *Neurology*. 2010;75:230-238.
27. Rabinovici GD, Rosen HJ, Alkalay A, et al. Amyloid vs FDG-PET in the differential diagnosis of AD and FTLD. *Neurology*. 2011;77:2034-2042.

28. Sled JG, Zijdenbos AP, Evans AC. A nonparametric method for automatic correction of intensity nonuniformity in MRI data. *IEEE Trans Med Imaging*. 1998;17:87-97.
29. Collins DL, Neelin P, Peters TM, Evans AC. Automatic 3D intersubject registration of MR volumetric data in standardized Talairach space. *J Comput Assist Tomogr*. 1994;18:192-205.
30. Zijdenbos AP, Forghani R, Evans AC. Automatic “pipeline” analysis of 3-D MRI data for clinical trials: application to multiple sclerosis. *IEEE Trans Med Imaging*. 2002;21:1280-1291.
31. Tohka J, Zijdenbos A, Evans A. Fast and robust parameter estimation for statistical partial volume models in brain MRI. *Neuroimage*. 2004;23:84-97.
32. Kim JS, Singh V, Lee JK, et al. Automated 3-D extraction and evaluation of the inner and outer cortical surfaces using a Laplacian map and partial volume effect classification. *Neuroimage*. 2005;27:210-221.
33. Joshi A, Koeppe RA, Fessler JA. Reducing between scanner differences in multi-center PET studies. *Neuroimage*. 2009;46:154-159.
34. Lyttelton O, Boucher M, Robbins S, Evans A. An unbiased iterative group registration template for cortical surface analysis. *Neuroimage*. 2007;34:1535-1544.
35. Friedman JH. Regularized Discriminant Analysis. *J Am Stat Assoc*. 1989;84:165-175.
36. Nichols TE, Holmes AP. Nonparametric permutation tests for functional neuroimaging: a primer with examples. *Hum Brain Mapp*. 2002;15:1-25.
37. Clark CM, Pontecorvo MJ, Beach TG, et al. Cerebral PET with florbetapir compared with neuropathology at autopsy for detection of neuritic amyloid- β plaques: a prospective cohort study. *Lancet Neurol*. 2012;11:669-78.
38. Waragai M, Okamura N, Furukawa K, et al. Comparison study of amyloid PET and voxel-based morphometry analysis in mild cognitive impairment and Alzheimer’s disease. *J Neurol Sci*. 2009;285:100-108.
39. Perani D, Schillaci O, Padovani A, et al. A Survey of FDG-and Amyloid-PET Imaging in Dementia and GRADE Analysis. *Biomed Res Int*. 2014; (Article ID 785039):22 pages.



The iteration process stops when the relabeling remains stable

Figure 1. Flow diagram of the automated, iterative process for classification of subjects according to β -amyloid level.

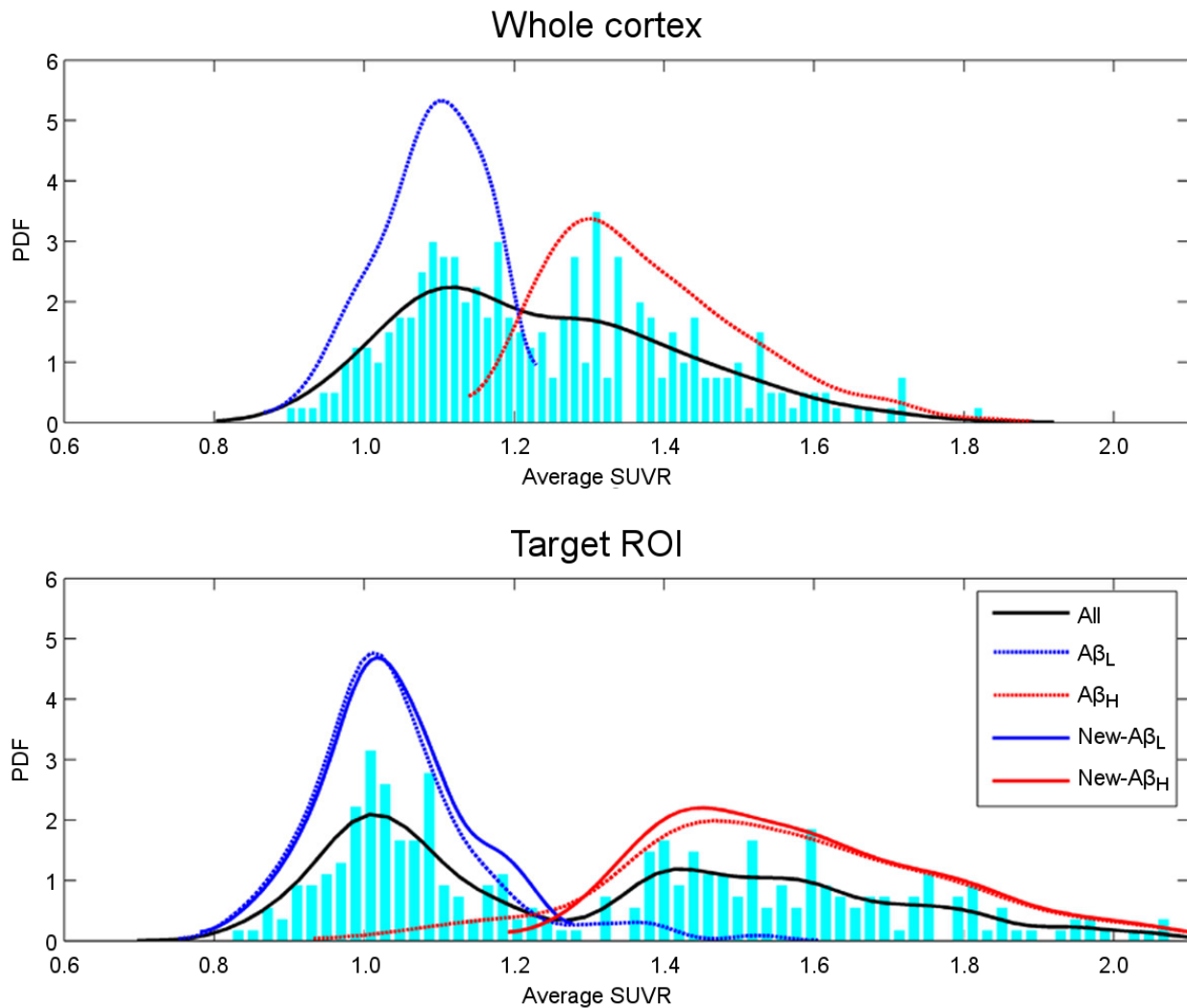


Figure 2. (Top) Distribution and estimated probability density function of the whole cortex $SUVR_{wc}$ values. RDA combined with ROC analysis initially separated Cohort 1 into two groups of 131 $A\beta_L$ and 145 $A\beta_H$ subjects. (Bottom) Distribution and estimated probability density function of the target ROI SUVR values obtained during four iterations of the automated discrimination process. All refers to the mean of all subjects, $A\beta_L$ and $A\beta_H$ correspond to the initial classification, and New- $A\beta_L$ and New- $A\beta_H$ correspond to the definitive classification based on the $SUVR_{ROI}$ values in the optimal target ROI.

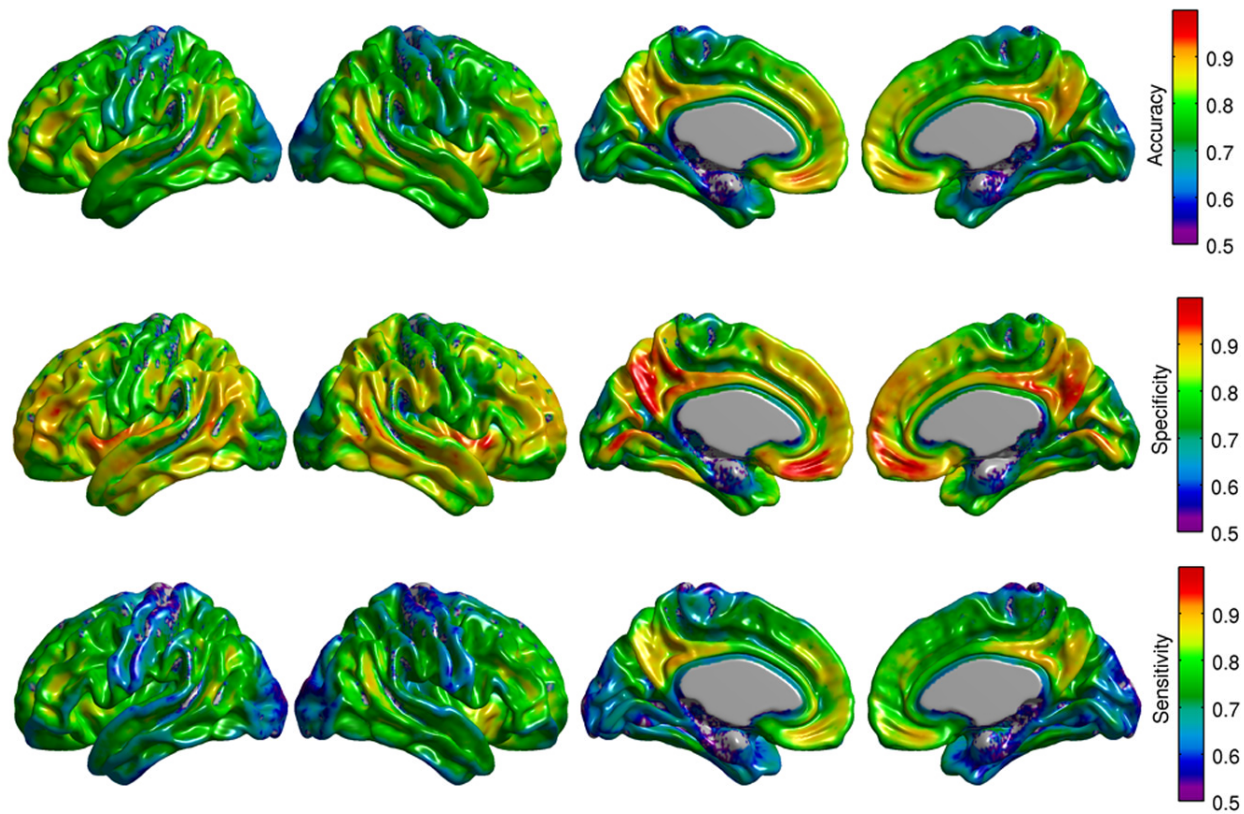


Figure 3. Cortical surface representation of the unthresholded maps of accuracy, specificity, and sensitivity following one iteration of voxelwise RDA.

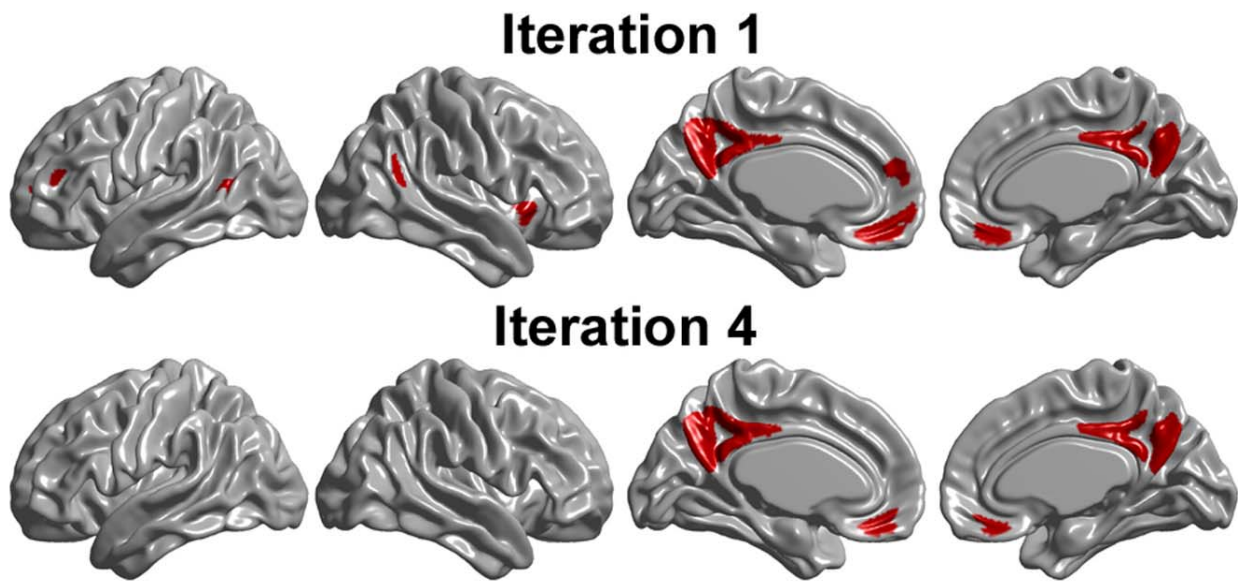


Figure 4. Target ROIs resulting from the initial and final iterations of the voxelwise RDA. The final, optimal target ROI includes bilateral regions of the precuneus and medial frontal cortex. A cutoff SUVR value of 1.24 for the average of the optimal target ROI separated Cohort 1 into two groups of 135 $A\beta_L$ and 141 $A\beta_H$ subjects.

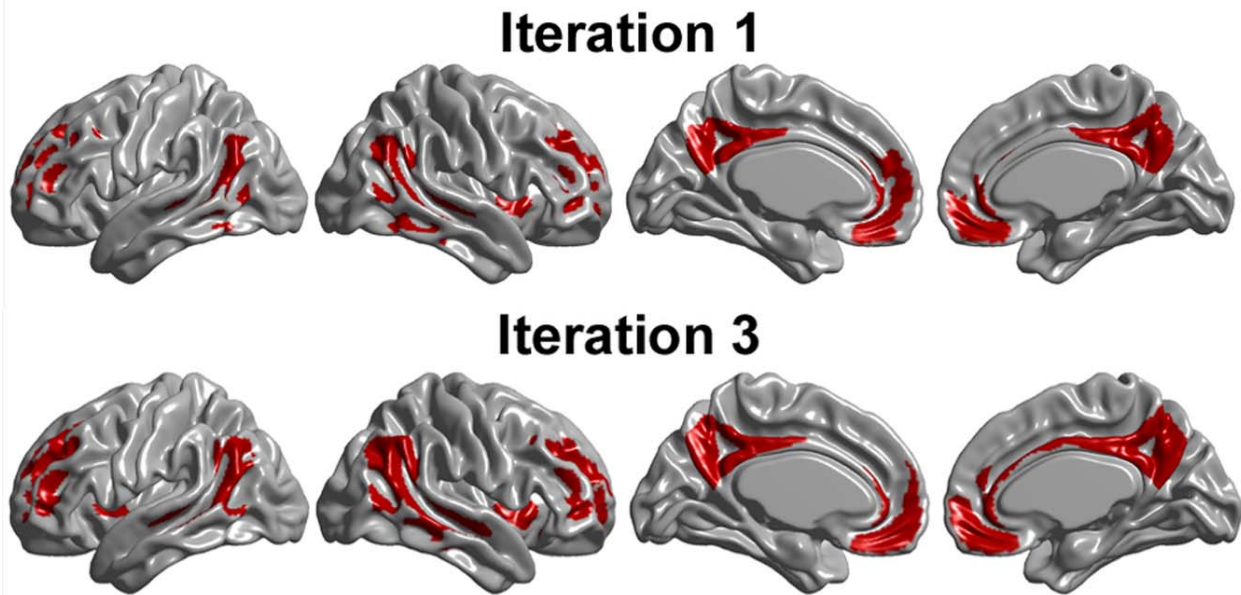


Figure 5. Target ROIs resulting from the initial and final iterations of the voxelwise RDA on Cohort 2. The final, optimal target ROI includes bilateral regions of the precuneus, medial frontal cortex, and temporal-parietal cortex.

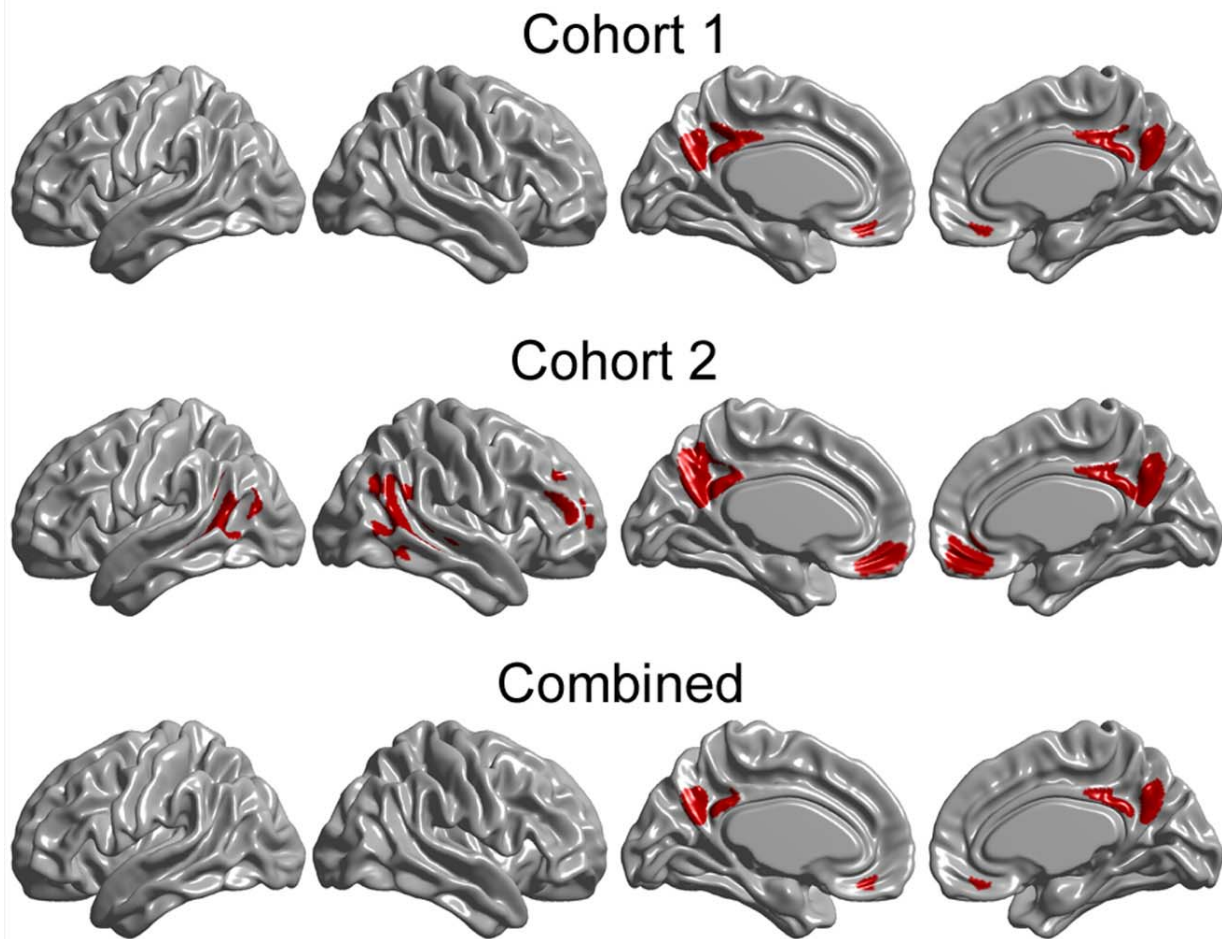


Figure 6. (Top and middle) Target ROIs resulting from the intersection of the target ROIs from different reference regions. (Bottom) Stable target ROI common to both cohorts.

	Cohort 1-EMCI	Cohort 1-LMCI	Cohort 2-NC	Cohort 2-AD
Sample Size	151	125	155	23
SUVR_{WC}	1.21 ± 0.17	1.28 ± 0.18	1.17 ± 0.15	1.36 ± 0.20
Age	71.28 ± 7.71	74.71 ± 7.89	76.74 ± 6.26	74.61 ± 10.95
Gender (F/M)	66/85	53/72	81/74	9/14
APOE ε4 (Carrier/Non-Carrier)	65/86	67/58	43/112	16/7
MMSE	28.45 ± 1.49	26.01 ± 4.19	28.93 ± 1.31	22.78 ± 2.08
ADAS-Cog	12.40 ± 5.24	21.52 ± 10.96	9.49 ± 4.58	30.82 ± 8.67
Sample Size CSF	136	88	111	21
CSF-Aβ₁₋₄₂ (pg/ml)	183.21 ± 49.94	154.90 ± 46.02	189.62 ± 52.38	146.72 ± 52.03

Table 1. Summary of subject characteristics.

	<u>Iter-0</u>	<u>Iter-1</u>	<u>Iter-2</u>	<u>Iter-3</u>	<u>Iter-4</u>
Cutoff	1.20	1.27	1.26	1.25	1.24
N_H	145	149	142	141	141
N_L	131	127	134	135	135
Acc-WC	0.985	0.960	0.949	0.945	0.949
Spec-WC	0.992	0.946	0.962	0.962	0.962
Sens-WC	0.979	0.972	0.937	0.931	0.938
Acc-Iter		0.960	0.975	0.996	1.000
Spec-Iter		0.946	1.000	1.000	1.000
Sens_Iter		0.972	0.953	0.992	1.000

Table 2. Sample size distribution, optimal cutoff values, and discrimination parameters obtained during the automatic iterative process applied to Cohort 1. At each iteration, accuracy, specificity, and sensitivity are calculated with respect to the initial classification at iteration 0 (Acc-WC, Spec-WC, and Sens-WC), and with respect to the preceding iteration (Acc-Iter, Spec-Iter, and Sens-Iter).

	Cohort 1-Aβ_L	Cohort 1-Aβ_H	Cohort 2-Aβ_L	Cohort 2-Aβ_H
Sample Size	135	141	108	70
SUVR_{ROI}	1.03 \pm 0.08	1.58 \pm 0.18	1.14 \pm 0.06	1.58 \pm 0.17
MMSE	28.19 \pm 2.48	26.53 \pm 3.68	28.90 \pm 1.49	26.95 \pm 3.23
ADAS-Cog	12.81 \pm 6.65	20.01 \pm 10.37	9.32 \pm 4.86	16.77 \pm 11.49
Sample Size CSF	116	108	75	57
CSF-Aβ₁₋₄₂ (pg/ml)	207.98 \pm 41.32	133.54 \pm 23.19	215.31 \pm 41.58	140.01 \pm 37.05

Table 3. Summary of clinical outcomes and CSF biomarkers in A β _L and A β _H groups.



The Journal of
NUCLEAR MEDICINE

Optimal Target Region for Subject Classification based on Amyloid PET Images

Felix Carbonell, Alex P. Zijdenbos, Arnaud Charil, Marilyn Grand'Maison and Barry Bedell

J Nucl Med.

Published online: July 1, 2015.

Doi: 10.2967/jnumed.115.158774

This article and updated information are available at:

<http://jnm.snmjournals.org/content/early/2015/07/01/jnumed.115.158774>

Information about reproducing figures, tables, or other portions of this article can be found online at:

<http://jnm.snmjournals.org/site/misc/permission.xhtml>

Information about subscriptions to JNM can be found at:

<http://jnm.snmjournals.org/site/subscriptions/online.xhtml>

JNM ahead of print articles have been peer reviewed and accepted for publication in *JNM*. They have not been copyedited, nor have they appeared in a print or online issue of the journal. Once the accepted manuscripts appear in the *JNM* ahead of print area, they will be prepared for print and online publication, which includes copyediting, typesetting, proofreading, and author review. This process may lead to differences between the accepted version of the manuscript and the final, published version.

The Journal of Nuclear Medicine is published monthly.
SNMMI | Society of Nuclear Medicine and Molecular Imaging
1850 Samuel Morse Drive, Reston, VA 20190.
(Print ISSN: 0161-5505, Online ISSN: 2159-662X)

© Copyright 2015 SNMMI; all rights reserved.

The logo for the Society of Nuclear Medicine and Molecular Imaging (SNMMI) consists of the letters 'S', 'N', 'M', and 'I' arranged in a 2x2 grid. Each letter is white and set within a red square. To the right of this grid, the full name of the society is written in a stacked, sans-serif font: 'SOCIETY OF NUCLEAR MEDICINE AND MOLECULAR IMAGING'.